

Review

Fundamental Mechanisms for Irradiation-Hardening and Embrittlement: A Review

Xiazi Xiao

Department of Mechanics, School of Civil Engineering, Central South University, Changsha 410075, China; xxz2017@csu.edu.cn; Tel.: +86-185-6949-9345

Received: 7 October 2019; Accepted: 17 October 2019; Published: 22 October 2019



Abstract: It has long been recognized that exposure to irradiation environments could dramatically degrade the mechanical properties of nuclear structural materials, i.e., irradiation-hardening and embrittlement. With the development of numerical simulation capability and advanced experimental equipment, the mysterious veil covering the fundamental mechanisms of irradiation-hardening and embrittlement has been gradually unveiled in recent years. This review intends to offer an overview of the fundamental mechanisms in this field at moderate irradiation conditions. After a general introduction of the phenomena of irradiation-hardening and embrittlement, the formation of irradiation-induced defects is discussed, covering the influence of both irradiation conditions and material properties. Then, the dislocation-defect interaction is addressed, which summarizes the interaction process and strength for various defect types and testing conditions. Moreover, the evolution mechanisms of defects and dislocations are focused on, involving the annihilation of irradiation defects, formation of defect-free channels, and generation of microvoids and cracks. Finally, this review closes with the current comprehension of irradiation-hardening and embrittlement, and aims to help design next-generation irradiation-resistant materials.

Keywords: irradiation-hardening; irradiation embrittlement; fundamental mechanisms

1. Introduction

Over recent decades, irradiation-hardening and embrittlement have been widely observed in nuclear structural materials with different crystalline structures [1–4], e.g., face-centered cubic (FCC) [5–8], body-centered cubic (BCC) [9–11] and hexagonal close-packed (HCP) [12–15] materials. Compared with their unirradiated counterparts, the yield stress or hardness of irradiated materials tends to increase with the irradiation dose (see Figure 1a,b for instance) until the density of irradiation-induced defects gets saturated. However, irradiation embrittlement, characterized by the decrease of elongation, reduction of fracture toughness and increase of the ductile to brittle transition temperature (DBTT) (see Figure 1c,d for example), originates from the effect of irradiation defects on the original failure mode of unirradiated metals.

The study of irradiation-hardening and embrittlement is non-trivial as it intrinsically denotes a typical multi-scale problem [16–19]. Under exposure to high-energy particles, lattice atoms in the pristine materials are displaced from their original sites, which further interact with the surrounding matrix that result in the formation of the so-called collision cascade, and after its cooling, a number of point defects such as interstitials and vacancies are recombined. The remaining point defects aggregate to form defect clusters that are visible under transmission electron microscopy (TEM), e.g., dislocation loops (DLs), stacking fault tetrahedra (SFTs) and voids [20]. In this way, the impact of high-energy particles at atomic scale leads to the formation of irradiation defects at micro scale [21,22]. With plastic deformation, these micro-scale defects not only act as obstacles impeding the movement of sliding dislocations but also get annihilated with the evolution of dislocations, which macroscopically affect

the mechanical behavior of irradiated metals [23,24]. With the development of numerical simulation capability and advanced experimental equipment, the mysterious veil covering the fundamental mechanisms of irradiation-hardening and embrittlement has been gradually unveiled in recent years.

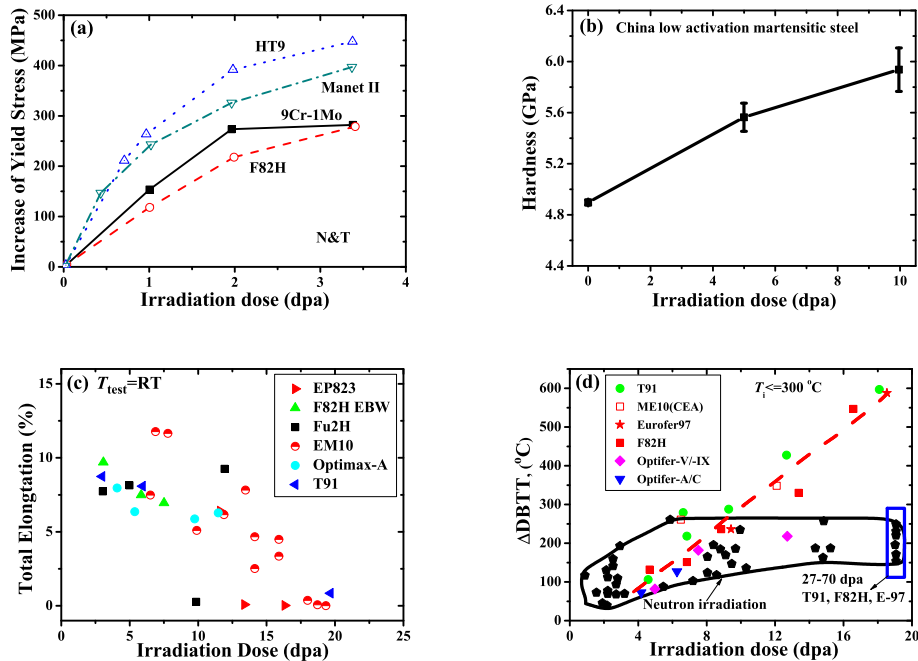


Figure 1. (color online) (a) Increase of the yield stress as a function of irradiation dose for reduced activation and conventional steels irradiated and tested at 698 K. (Reprinted with permission from [4]. Copyright 2000 by Elsevier.) (b) Hardness as a function of irradiation dose for nanocrystalline CLAM steels irradiated by Xe ions at room temperature (Reprinted with permission from [25]. Copyright 2014 by Elsevier.) (c) Total elongation as a function of irradiation dose for ferritic/martensitic steels when irradiated at 623 K in STIP and 598 K in BOR60. (Reprinted with permission from [26]. Copyright 2011 by Elsevier.) (d) Change of DBTT as a function of irradiation dose for ferritic/martensitic steels irradiated in fission reactors and STIP. (Reprinted with permission from [26]. Copyright 2011 by Elsevier.)

Numerical simulation of the irradiation effect on mechanical degradation at various spatial and temporal scales needs a combination of different approaches, e.g., *ab-initio* calculations [27,28], molecular dynamics [29–33], dislocation dynamics [34–36], and finite element simulation [37–40], etc. At atomic scale, it has become convenient to study the fundamental mechanisms related to the generation and evolution of irradiation defects, as well as their interaction with dislocations and microstructures under different irradiation conditions, which can be compared with the experimental observations at macro scale for both irradiation-hardening and embrittlement [29,35,38]. For instance, it has been indicated by Bacon et al. [41,42] that the comprehensive study of the dislocation-defect interaction can be effectively investigated by atomistic simulations either in static ($T = 0$ K) or in dynamic ($T > 0$ K) conditions. Static modelling offers information that can be directly compared with the one obtained from the elasticity theory of dislocations, as it provides the equilibrium configuration at a given stress or strain. Dynamic simulation makes it available to address the temperature effect on the interaction and evolution mechanisms between dislocations and defects that depend on material properties, dislocation characters, morphologies of defects, and simulation conditions [43–45]. In addition, recent research progress indicates that the establishment of a multi-scale hierarchical method is critically important for the simulation of collision cascades, diffusion of point defects and

their clustering, dislocation movement and dislocation-defect interaction, and mechanical testing of irradiated materials including uniaxial tension and nano-indentation [46–49].

On the other hand, experimental observation and test offer the most reliable data for the analysis of irradiation-hardening and embrittlement. The informed knowledge ranges from the formation of irradiation-induced defects at nano scale [50–52], to the generation of defect-free channels within the grain interiors and across adjacent grains at micro scale [53,54], to the stress-strain relationship, hardness-depth curve and fracture toughness-temperature relationship at macro scale [55–59]. It can also provide the information for the type, distribution and density of irradiation defects at the static state [60,61], and the dynamic interaction between dislocations and defects during the irradiation and loading process [62,63]. The observation of irradiation-induced defects by advanced experimental techniques, and their interaction with gliding dislocations detected by in situ experiments could tremendously enrich our understanding of the plastic deformation in irradiated materials. In addition, the measured density and size of irradiation defects can be adopted as the input parameters for numerical simulations and theoretical models [37,38,64].

Informed by the numerical simulations and experimental observations over recent decades, the fundamental mechanisms related to irradiation-hardening and embrittlement are reviewed in this work, which intends to offer an effective guidance for the design of irradiation-resistant materials. The outline of this review is organized as follows: in Section 2, the formation of irradiation-induced defects is discussed, which covers the influence of both irradiation conditions and material properties. In the following, the interaction between dislocations and irradiation defects is addressed, including the summary of both the interaction process and strength for different defect types and testing conditions. In Section 4, the evolution details of defects and dislocations are focused on, involving the annihilation of irradiation defects, formation of defect-free channels and generation of microvoids and cracks. Summary and outlook messages are collected in Section 5.

2. Formation of Irradiation-Induced Defects

Intrinsically speaking, both irradiation-hardening and embrittlement are affected by irradiation-induced defects. The formation and growth of irradiation-induced defects are a complex process that is determined by both irradiation conditions and material properties. The former includes the irradiation temperature, irradiation dose and flux, etc.; and the latter involves the crystalline structures, stacking fault energy, chemistry, and so on [65–68]. A summary of the dominant irradiation defects observed in different types of nuclear structural materials is listed in Table 1.

Table 1. The dominant irradiation-induced defects observed in different types of nuclear structural materials.

Materials	Dominant Defects	Irradiation Conditions
Copper [69]	SFTs	0.8 dpa and 343 K with neutrons
Copper [7]	DLs and SFTs	0.001–0.1 dpa and 353–423 K with neutrons
Nickel alloy [70]	DLs	Up to 82.5 dpa and 293 K with 115 KeV argon ions
Nanocrystalline Ni [8]	DLs	Up to $2.3 \times 10^{16}/\text{cm}^2$ and 293 K with 12 MeV He ions
Iron [10]	DLs	0.8 dpa and 343 K with neutrons
Iron [9]	DLs	0.375 dpa and 523 K with neutrons
Tungsten [11]	Voids, bubbles and DLs	0.15–0.47 dpa and 804–1073 K with neutrons
Tungsten [71]	DLs	0.006–0.03 dpa and 363 K with neutrons
Palladium [60]	DLs	0.12 dpa and 320 K with 590 MeV protons

Table 1. Cont.

Materials	Dominant Defects	Irradiation Conditions
ODS steels [72]	DLs	1 dpa and 623 K with 590 MeV protons
EUROFER ODS steels [73]	DLs	16.3 dpa and 298–723 K with neutrons
Reduced-activation steels [74]	Precipitates	5 dpa and 623 K with neutrons
T91 steels [75]	DLs	0.06 dpa and 573 K with neutrons
EUROFER97 steels [75]	DLs	1.5 dpa and 573 K with neutrons
EUROFER97 steels [76]	DLs, voids and helium bubbles	16.3 dpa and 523–723 K with neutrons
Fe-Cr alloys [61]	DLs and solute rich clusters	0.06–1.5 dpa and 433–573 K with neutrons
Fe-Cr alloys [77]	DLs	8 MeV and 293 K with Fe ions
304 and 316 austenitic stainless steels [78]	DLs	0.36–5 dpa and 623 K with 160 KeV Fe ions
RAFM steels [79]	DLs	He 23 appm/dpa and 673 K
HT-9 steels [80]	DLs	$8 \times 10^{20}/\text{cm}^2$ and 573–773 K with 14 MeV nickel ions
F82H steels [81]	DLs and Helium bubbles	10.7–19.6 dpa and 438–578 K with He
CLAM steels [52]	DLs	3×10^{16} ion/cm ² and 773 K with He ⁺ ions
Molybdenum [82]	DLs	0.28 dpa and 353 K with neutrons

2.1. Irradiation Condition

Irradiation conditions evolve during the service process of nuclear structural materials in fission and fusion reactors. The experimental characterization of irradiation-induced defects, including their type, density and distribution, is possible only out of operation [83–86]. For instance, as one of the most promising first wall materials, tungsten should suffer from the impact of both high energetic neutrons and plasma ions, which results in the generation of irradiation defects and local stresses in the plasma facing components. With the increase of irradiation time, both the irradiation dose and plastically deformed region increase that affect the distribution and density of irradiation-induced defects. In the following, three dominant factors related to the irradiation condition are discussed, including the irradiation dose, irradiation temperature and irradiation particle.

(1) Irradiation dose. In general, the irradiation dose is characterized by the fluence of particles per unit area, which can be converted to dpa (NRT). With the increase of irradiation dose, a increasing number of point defects are generated during the collision cascades that finally result in the increase of the density of defect clusters until it gets saturated (as shown in Figure 2). At moderate to high irradiation dose, these defect clusters with a saturated density further aggregate to form voids at the nano scale. Compared to the evolution tendency of the cluster density, the size of irradiation-induced defects seems to be less sensitive to the irradiation dose, and almost keeps at a constant value with the increase of irradiation dose for most nuclear materials [61,75].

(2) Irradiation temperature. The formation and growth of defect clusters are closely related to the ambient temperature as the re-emission of interstitials or vacancies from defect clusters is a thermally activated process. The growth of defect clusters occurs when the irradiation temperature is sufficiently high for the diffusion of irradiation defects. However, increasing the irradiation temperature beyond a certain limit will result in the emission of point defects from the clusters, which further promotes the recombination of point defects, and reduces the density of defect clusters (e.g., DLs and SFTs) [12,87,88]. The existence of the peak in the void swelling vs. irradiation temperature is a classical example of these two counteracting processes. For instance, as presented in Figure 3, the size of irradiation-induced voids as observed in neutron-irradiated molybdenum alloys was found to be strongly dependent on the irradiation temperature [89]. With the increase of the temperature from 573 K to 1173 K, the observed

defects evolve from fine voids (with the diameter D around 1 nm) to moderate ones ($D = 5\text{--}6$ nm) to large ones ($D = 8\text{--}30$ nm). Meanwhile, the number density of voids gradually decreases with the increase of void size.

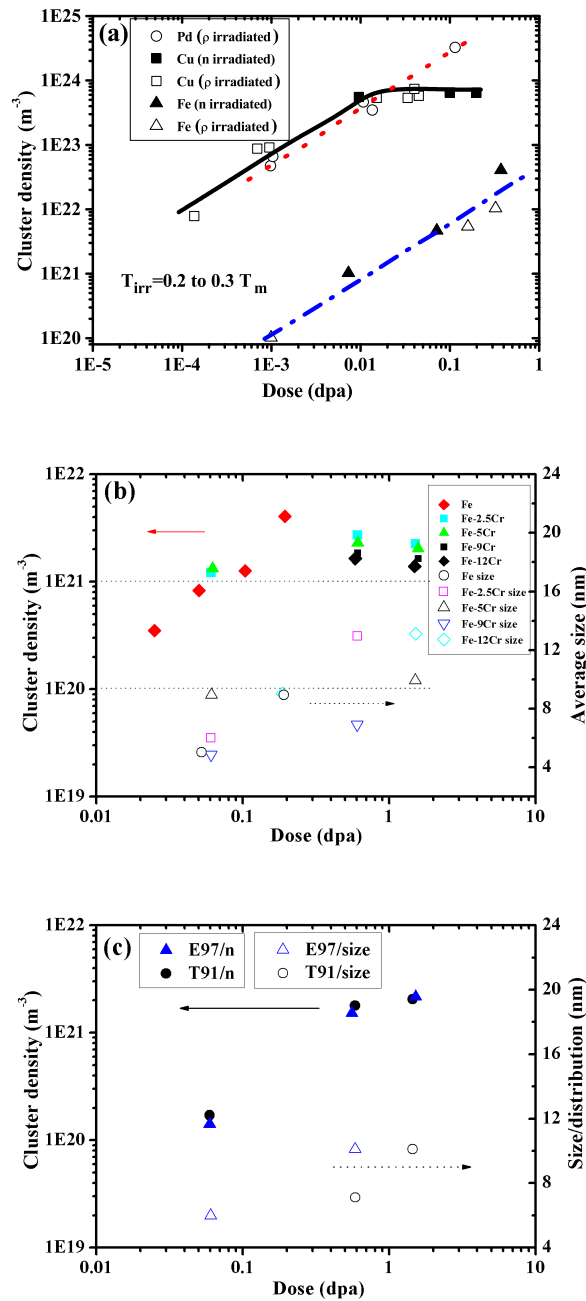


Figure 2. (color online) Dose dependence of cluster density and size distribution under neutron or proton irradiation. (a) Cu, Pd and Fe. (Reprinted with permission from [60]. Copyright 2000 by Elsevier.) (b) Fe and Fe-Cr alloys. (Reprinted with permission from [61]. Copyright 2008 by Elsevier.) (c) T91 and EUROFER97 steels. (Reprinted with permission from [75]. Copyright 2008 by Elsevier.)

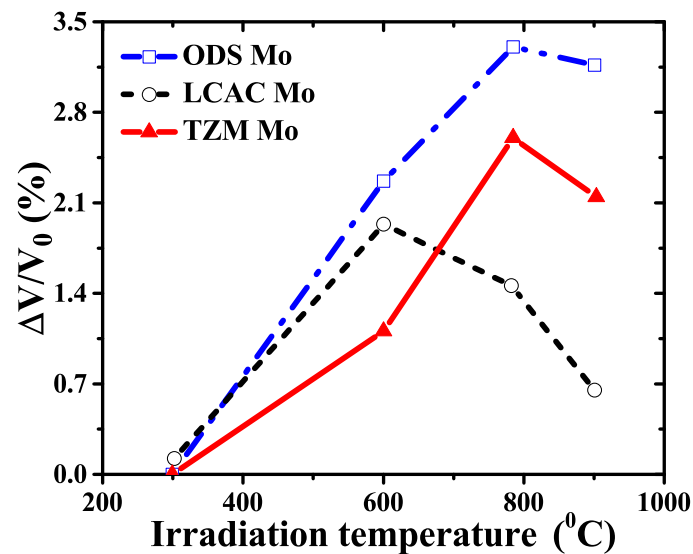


Figure 3. (color online) Maximum swelling as a function of irradiation temperature for oxide dispersion strengthened (ODS), low carbon arc cast (LCAC) and molybdenum-0.5pct titanium-0.1pct zirconium (TZM) molybdenum under highest fluence. (Reprinted with permission from [89]. Copyright 2011 by Elsevier.).

(3) Irradiation particle. Due to the different energy spectra of irradiation particles, their interaction mechanism with crystalline atoms may not necessarily be the same, which results in various distribution profiles of defect density within the irradiated materials. For instance, under neutron irradiation, the irradiated materials can be easily got through by neutrons (given the typical dimension of in-vessel nuclear components), which makes the irradiation-induced damage profile be uniformly distributed throughout the whole component. As a comparison, for the case of ion irradiation, the generated defects are usually within the shallow region (up to a few micrometers) because of the limited penetrating capacity of ions, and the defect distribution is non-uniform making standardized mechanical testing almost inapplicable [52,64,90,91]. Though the distribution of irradiation-induced defects might not be the same for neutron and ion irradiation, the dominant defect type is usually identical, which mainly depends on the crystalline structure and irradiation temperature.

To conclude, the formation of irradiation-induced defects is very sensitive to the irradiation condition even for the same irradiated materials. Therefore, the comprehension analysis of defect formation during the irradiation experiments is very important for the further interpretation of microstructures and assessment of mechanical properties.

2.2. Material Properties

As an intrinsic factor, the material properties of nuclear structural materials, including the type of crystalline structures and content of alloying elements, are critically important in determining the formation of irradiation-induced defects as informed in both experimental and computational studies [92–96].

Generally speaking, the dominant irradiation defects formed in metallic materials with different crystalline structures are not necessary the same (as summarized in Table 1). At moderate irradiation conditions, SFTs are the most widely observed defects in FCC metals [7,69,97], whereas, in BCC and HCP materials, the dominant defects are DLs [14,71,72]. With the increase of irradiation temperature and dose, voids gradually become dominant in all FCC, BCC and HCP materials. Moreover, the distribution of these irradiation-induced defects within the grain interiors has their characteristic features. For instance, the habit planes of SFTs, i.e., {111} planes, coincide with the dislocation slip

planes of $\{111\}\langle 110\rangle$ slip systems in FCC metals. In BCC metals, DLs acquire the habit planes of $\{111\}$ or $\{110\}$ or $\{100\}$ depending on the direction of the Burgers vector of DLs [98]. For HCP metals, most irradiation-induced DLs are located on the basal plane, resulting in the non-uniform distribution of defects on different slip systems.

The addition of alloying elements and impurity atoms not only affects the mechanical properties of pure metals, but also modifies the morphology and size/density distribution of irradiation-induced defects. For instance, the dominant defects observed in irradiated Fe-Cr alloys include not only DLs but also solute rich clusters, which consist of major alloying element Cr and minor alloy elements such as P and Si, etc. These two kinds of defects are found to be equally important to characterize the hardening behavior of irradiated Fe-Cr alloys. Moreover, the interaction between alloying elements and point defects can promote the generation of non-equilibrium configurations including the segregation and depletion around the grain boundaries (see Figure 4) [22,99–101].

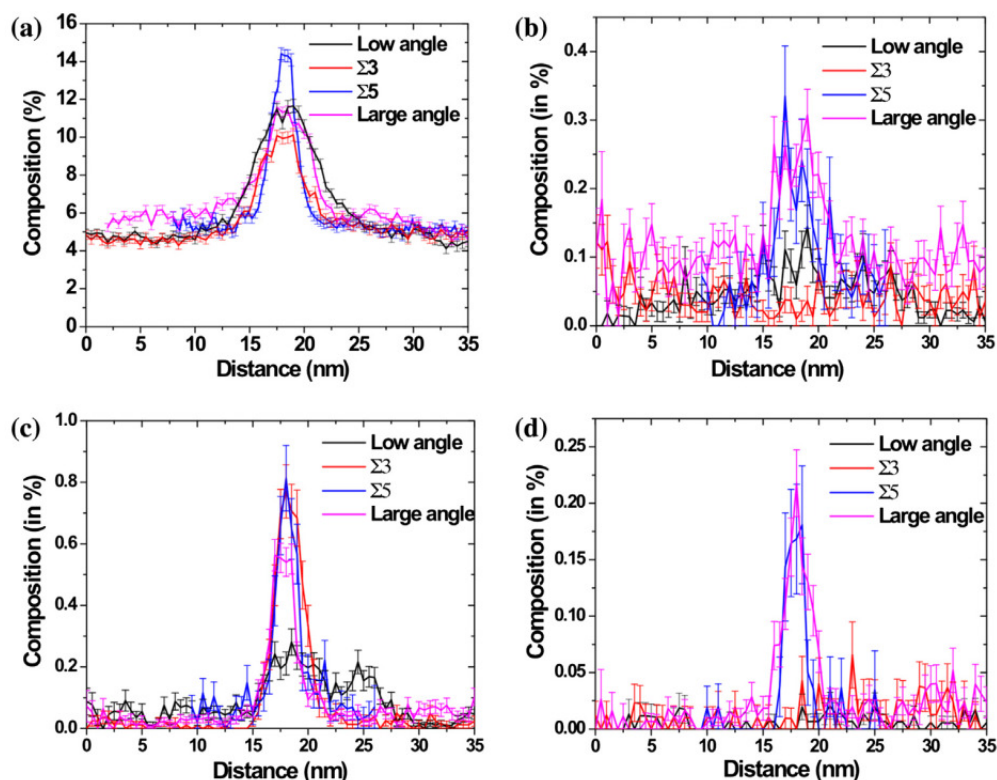


Figure 4. (color online) Distribution profiles of (a) Cr, (b) C, (c) Si and (d) P concentration across different types of grain boundaries for neutron-irradiated Fe-6%Cr alloys. (Reprinted with permission from [99]. Copyright 2014 by Elsevier.).

Besides the influence of crystalline structures and alloy elements, there are other strategies such as the interface engineering that can affect both the formation and distribution of irradiation-induced defects [8,92,95,96,102]. A systematical study of these intrinsic influence factors could be a promising strategy that shines light on the way for the design of irradiation-resistant materials in the near future.

3. Interaction between Defects and Dislocations

Compared to the glissile dislocations, which can move under external applied load, irradiation-induced defects are usually sessile (except perfect DLs who indeed have very low migration energy). Therefore, the dislocation-defect interaction can be taken as the contact between a series of gliding dislocations and fixed defect obstacles, which eventually results in irradiation-hardening [103]. Meanwhile, this interaction process strongly depends on the spatial contact position, and the interaction strength is determined by the defect type, dislocation character, test temperature and loading rate, etc.

3.1. Interaction Process

The way how dislocations interact with irradiation defects is a complex process, which is closely related to their mutual spatial positions, as illustrated in Figure 5. In irradiated materials with crystalline structures, dislocations should glide on corresponding sliding planes. Moreover, the irradiation-induced defects also occupy certain specific habit planes, e.g., $\{111\}$ for DLs and SFTs [104,105]. Therefore, the dislocation-defect interaction can be classified into two general cases, i.e., the parallel interaction and non-parallel interaction, which depends on the mutual orientation relationship between the dislocation glide planes and defect habit planes.

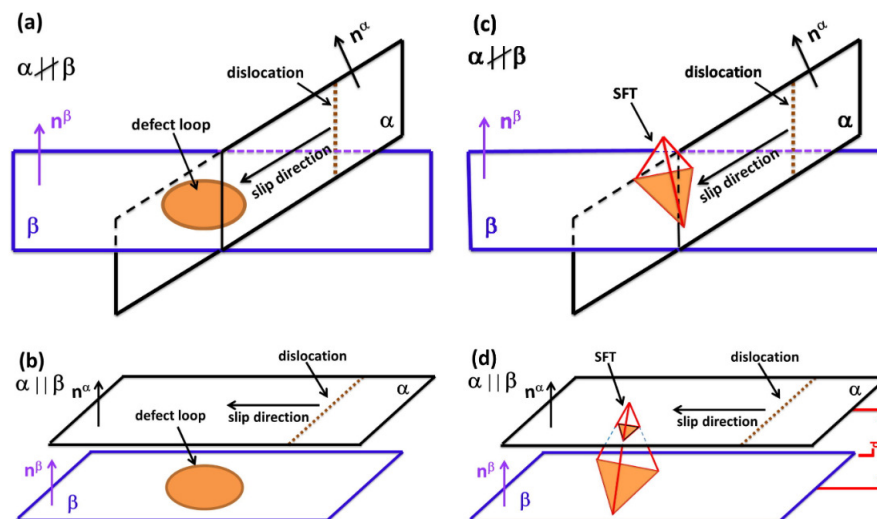


Figure 5. (color online) Illustration of the dislocation-DL and dislocation-SFT interaction when their slipping planes and habit planes are parallel or not. (a) The slipping plane of dislocations is not parallel to the habit plane of DLs; (b) the slipping plane of dislocations is parallel to the habit plane of DLs; (c) the slipping plane of dislocations is not parallel to the habit plane of SFTs; and (d) the slipping plane of dislocations is parallel to the habit plane of SFTs. (Reprinted with permission from [106]. Copyright 2015 by Elsevier.).

For the case of DLs, when the loop habit plane is parallel to the slip plane of dislocations, DLs can hardly interact with dislocations, which results in no hardening behavior and limited evolution of the density of defects. Here, the discussion concerns the direct dislocation-defect interaction, which excludes the long-range elastic interaction. Otherwise, DLs would act as obstacles impeding the sliding of mobile dislocations, which, on the one hand, leads to the irradiation-hardening, and on the other hand, results in the full or partial removal of DLs and formation of defect-free channels. The situation for SFTs is somewhat special because of the three-dimensional structure of SFTs. When the slip plane of dislocations is parallel to one of the habit planes of SFTs, the interaction may still occur depending on the distance between the dislocation slip plane and SFT habit plane relative to the height of SFTs. If the distance is larger than the height of SFTs, no interaction happens as in the case of the dislocation-DL interaction [38,107]. If not, the sliding dislocations can still contact with SFTs, which results in (1) the direction incorporation of SFTs on the dislocation line, or (2) truncation of SFTs with/without small SFTs, which depends on the size of SFTs, the type of dislocations and test temperature. As to the case of voids, the interaction is rather simple. At low test temperatures, voids are strong obstacles so that gliding dislocations pass by the emission and closure of the dipoles. The surmounted void is sheared and a characteristic step on the void surface is left after each interaction process. With the increase of the test temperature, surface climb and dislocation cross-slip are also activated such that several vacancies can be absorbed on the dislocation line after the interaction.

3.2. Interaction Strength

The interaction strength (or say the critical stress) for the transmission of dislocations through irradiation defects is determined by the defect morphology, test temperature and dislocation character, etc [22,108,109]. As observed in experiments, irradiation-induced defects can be categorized into four types: point defects (e.g., interstitials and vacancies), one-dimensional defects (e.g., dislocations), two-dimensional defects (e.g., DLs), and three-dimensional defects (e.g., SFTs, voids, solute rich clusters, and precipitates) [22,110]. Besides point defects, the rest irradiation-induced defects can all, to some extent, impede the movement of sliding dislocations. Among them, voids can hardly be annihilated by sliding dislocations, which reveals the strongest interaction strength when compared with the rest type of defects. The interaction strength induced by DLs and SFTs is moderate, therefore, defect-free channels can be observed in irradiated materials with the subsequent annihilation of these two types of defects. It should be noted that screw dislocations tend to cross-slip when encountered with the impediment of sessile defects [111], therefore, in general, the interaction strength for screw dislocations differs from that of edge dislocations.

Test temperature is also an important factor affecting the interaction strength [109]. Based on the Orwan theory, the interaction strength induced by the regular square array of defects can be expressed as $\tau = h_d \mu b \sqrt{N_{\text{def}} d_{\text{def}}}$ with h_d the defect strength coefficient, μ the shear modulus, b the magnitude of the Burgers vector, N_{def} the numerical density of defects and d_{def} the average size of defects. For a given density and size of irradiation defects, it is found that h_d decreases with the increase of test temperature for neutron-irradiated Cu [7], which indicates that the interaction strength gradually vanishes with the increase of test temperature, as shown in Figure 6. This is explained by the thermally activated nature of the interaction between dislocations and irradiation-induced defects.

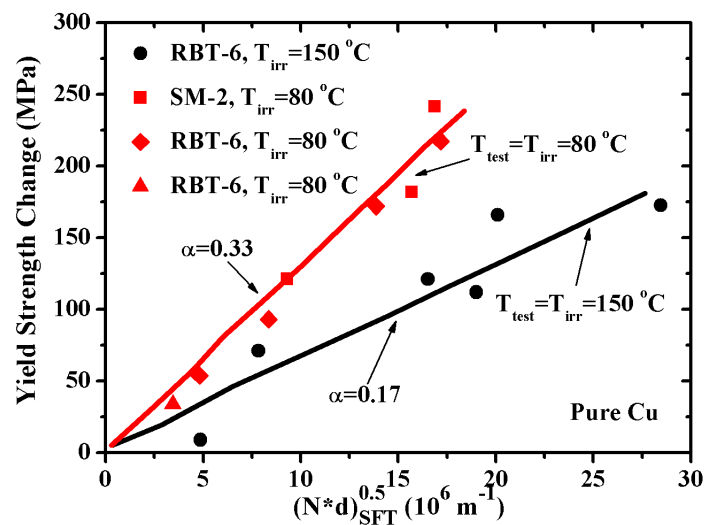


Figure 6. (color online) Temperature effect on the irradiation-hardening coefficient α of pure Cu under neutron irradiation. (Reprinted with permission from [7]. Copyright 2007 by Elsevier.).

4. Evolution of Defects and Dislocations

During the plastic deformation process, the persistent dislocation-defect interaction could result in the evolution of irradiation defects and dislocations is responsible for the irradiation embrittlement. In general, the evolution of defects and dislocations can be categorized into three stages: the annihilation/removal of defects by sliding dislocations, formation of defect-free channels, and germination of microvoids and cracks. Thereinto, the annihilation/removal of defects comes from the persistent dislocation-defect interaction, which results in the incorporation of irradiation defects on

the dislocation lines. Therefore, formed defect-free channels offer the regions where the dislocation slip is easy, and this establishes the highly localized plastic deformation zone. Following that, microvoids tend to germinate around the intersection sites between the defect-free channels and grain boundaries with the accumulation of dislocations, which finally leads to the extension of cracks throughout the irradiated materials.

4.1. Annihilation of Defects

Defect annihilation/removal is a micro-scale phenomenon, and has long been in the mist due to the limitation of experimental observation technique and numerical simulation methods. Recently, with the development of TEM, the direct observation of the dislocation-defect interaction and the subsequent evolution of defects and dislocations have become available, which tremendously enriches our understanding of the dislocation-defect interaction at micro scale.

For instance, Figure 7 illustrates the in situ observation of the evolution of SFTs during the interaction process with sliding dislocations [62,63]. In Figure 7a, two SFTs respectively labeled “A” and “B” are indicated in irradiated gold, thereinto, a glissile dislocation gets physical interaction with SFT “B”, and results in the collapse of SFT “B” into a glissile DL and glides away. As a comparison, the other SFT named “A”, which is close to SFT “B” but does not interact with the sliding dislocation, remains unchanged [62]. This observation points out that the collapse of irradiation defects does not originate from the interaction stress field induced by dislocations and defects, but from the direct physical interaction, i.e., the dislocation-defect contact [63]. Figure 7b also captures the sequential interaction between three dislocations and one SFT [63]. These images prove that the defect annihilation may come from the sequential interaction with a series of sliding dislocations.

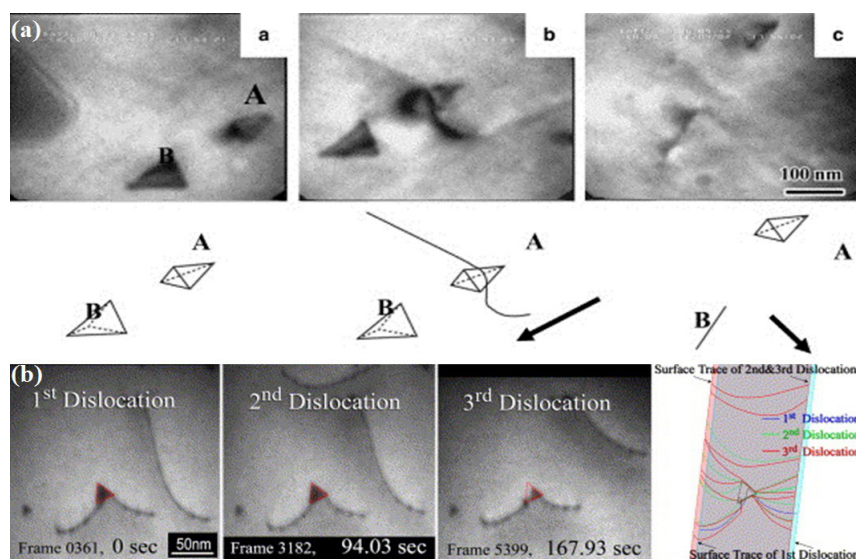


Figure 7. (color online) In situ observation of the annihilation of SFTs through the interaction with sliding dislocations. (a) The SFT labeled “B” collapses into a glissile dislocation with the remnant dislocation gliding away in gold. (Reprinted with permission from [62]. Copyright 2005 by Elsevier.) (b) The SFT is annihilated through a sequential interaction with sliding dislocations. (Reprinted with permission from [63]. Copyright 2004 by Elsevier.)

As a summary of the experimental observations, five different outcomes of the defect-dislocation interaction are revealed, namely: (1) Defects remain unaffected while the contacted dislocations slide away [111]. (2) Defects are completely absorbed with no influence on the gliding dislocations [112]. (3) Formation of a drag, either through the long-range elastic interaction or via the absorption of defects on dislocation lines in a form of superjog, which occurs for edge dislocations. The absorption of defects on the screw dislocation line creates helical turns that would pin the further movement

of dislocations, and therefore the helix should either be emitted (as perfect loops) or removed from the dislocation line by sliding along the line to the nearest sink (e.g., grain boundaries or voids) [113,114]. (4) The defect is transformed into other types, e.g., a SFT collapses into a Frank loop following the inverse Silcos-Hirsch mechanism [62,63,114] or a $\langle 100 \rangle$ loop is converted into a $a/2\langle 111 \rangle$ loop. (5) Defect is sheared by dislocations and remains as a single one or is broken into small ones [111,113,115,116]. These experimental observations could help verify the fundamental mechanisms observed in numerical simulations, and also provide insights into the formation of defect-free channels in irradiated materials [117].

4.2. Formation of Defect-Free Channels

A distinguished feature observed in irradiated materials is the formation of defect-free channels (or say dislocation channels) after plastic deformation [118] as illustrated in Figure 8. The dominant characters of defect-free channels involve the channel width (around $0.1 \mu\text{m}$), inter-channel spacing (about $1\text{--}3 \mu\text{m}$) and the amount of accumulated shear strain in channels [119,120]. Through measuring the step height on the surface of irradiated samples and the offset caused by the channel-grain boundary intersection, the amount of shear strain in channels is estimated to be about two orders of magnitude higher than that of bulk materials without irradiation effect [121].

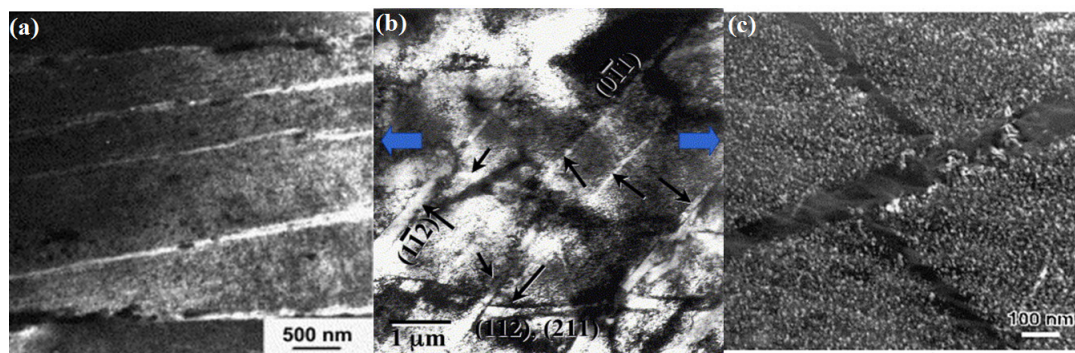


Figure 8. (color online) Observation of defect-free channels (or say dislocation channels) in irradiated metals after plastic deformation. (a) Zirconium alloys. (Reprinted with permission from [122]. Copyright 2004 by Elsevier.) (b) Iron irradiated at 0.4 dpa and 343 K. (Reprinted with permission from [10]. Copyright 2006 by Elsevier.) (c) Palladium single crystals irradiated with protons. (Reprinted with permission from [60]. Copyright 2000 by Elsevier.).

To uncover the formation process of defect-free channels, a number of experimental observations have been performed [10,60,118,122,123]. One representative experiment is the study of strain localization in irradiated 316 stainless steels when the temperature ranges from 323 K to 473 K. It is found that the formation of defect-free channels becomes dominant when the neutron irradiation dose reaches 0.78 dpa, and the channel width would gradually evolve with the growth of channels [118]. Moreover, the formation of defect-free channels is investigated in neutron-irradiated molybdenum. The experimental results indicate that the irradiation-induced DLs in molybdenum are unstable with respect to the external stress. The observation of the loop-loop interaction is believed to play a significant role in the early formation stage of defect-free channels [123]. As indicated in these experimental observations, the formation of defect-free channels is found to be related to the local grain orientation, Schmid factors, stacking fault energy and irradiation conditions, etc. [124].

Generally speaking, in the vicinity of grain boundary triple junctions, dislocations tend to be generated because of stress concentration [125]. These emitted dislocations from grain boundaries would interact with irradiation-induced defects in the grain interiors with high Schmid factors, which results in the annihilation of defects and formation of defect-free channels. It has also been indicated that the localized plastic deformation is suppressed in the materials with low stacking fault energy due to the limited number of active slip systems and low probability for cross-slip. However,

with the increase of irradiation doses, sufficient defects can ensure the dislocation-defect interaction, and therefore, defect-free channels are found to be general even in irradiated stainless steels with low stacking fault energy [124].

To explain the reason defect-free channels are formed with a certain width, two possible explanations have been put forward [110,111,126,127]: (1) Dislocation source widening at grain boundaries and stress concentration sites. As observed in irradiated 304 stainless steels, the dislocation source region is actually a volumetric element, and the emission of dislocations is a dynamic process that if one region is inhibited, a new nearby region can be activated as another dislocation source. This phenomenon may help explain the width of defect-free channels as the generated dislocations from these source regions are of the same type on parallel slip planes [110]. (2) Cross-slip of dislocations. According to the simulation results of dislocation dynamics (see Figure 9), it is pointed out that the formation of defect-free channels is strongly dependent on the cross-slip of dislocations when encountered by sessile defects [35,126]. In addition, the phenomenon of double cross-slip is observed in the SFT-dislocation interaction process that SFTs finally collapse into Frank loops [111]. However, it should be noted that cross-slip alone may not be sufficient to result in the formation of defect-free channels as observed in experiments. Moreover, it has been indicated that the width of channels increases with test temperature, indicating that the channel widening process should also involve a thermally activated mechanism [127].

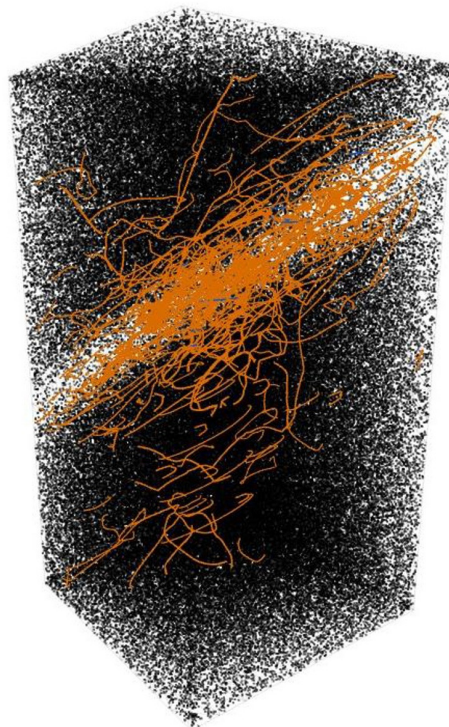


Figure 9. (color online) Distribution of irradiation defects and dislocation configurations when the irradiation dose equals 0.375 dpa for neutron-irradiated iron. Numerical results are performed by coupled Field-dislocation dynamics simulations. (Reprinted with permission from [35]. Copyright 2018 by Elsevier.).

4.3. Generation of Microvoids and Cracks

With the development of defect-free channels, the degree of localized deformation within channels becomes so high that the plastic deformation mainly occurs within the channels while the surrounding “matrix” remains undeformed. As soon as the in-channel dislocations hit the grain boundary, three types of the channel-grain boundary interaction are observed: (1) continuous slipping of dislocations across grain boundaries, (2) the absorption of sliding dislocations into grain boundaries leading to

the sliding of grain boundaries, and (3) the accumulation of dislocations around the vicinity of grain boundaries resulting in the establishment of stress concentration. Given the sufficient accumulation of dislocations in the pile-up region near the grain boundary and intensive inter-boundary slip, vacancies may start to generate as a result of stress concentration. The generation of those vacancies and their coalescence into clusters will eventually facilitate the germination of microvoids. The latter two mechanisms are believed to promote the nucleation of microvoids, while the coalescence of microvoids would result in the formation of cracks [128].

Actually, the formation of microvoids is likely to occur near the interaction sites of defect-free channels and grain boundaries. In the scanning electron microscopy image as illustrated in Figure 10a, it can be seen that the grain boundaries act as obstacles for the sliding of dislocations within the defect-free channels. Due to the pile-up of dislocations at grain boundaries, the local stress dramatically increases with the strain in the channel increasing up to 200% compared with the 2.5% macroscopic strain. Through the absorption of dislocations and continuous sliding of these dislocations along the grain boundary, stress concentration can be moderated to some extent. However, the formation of microvoids is inevitable due to the concentration of vacancies near the channel-grain boundary interaction regions [129].

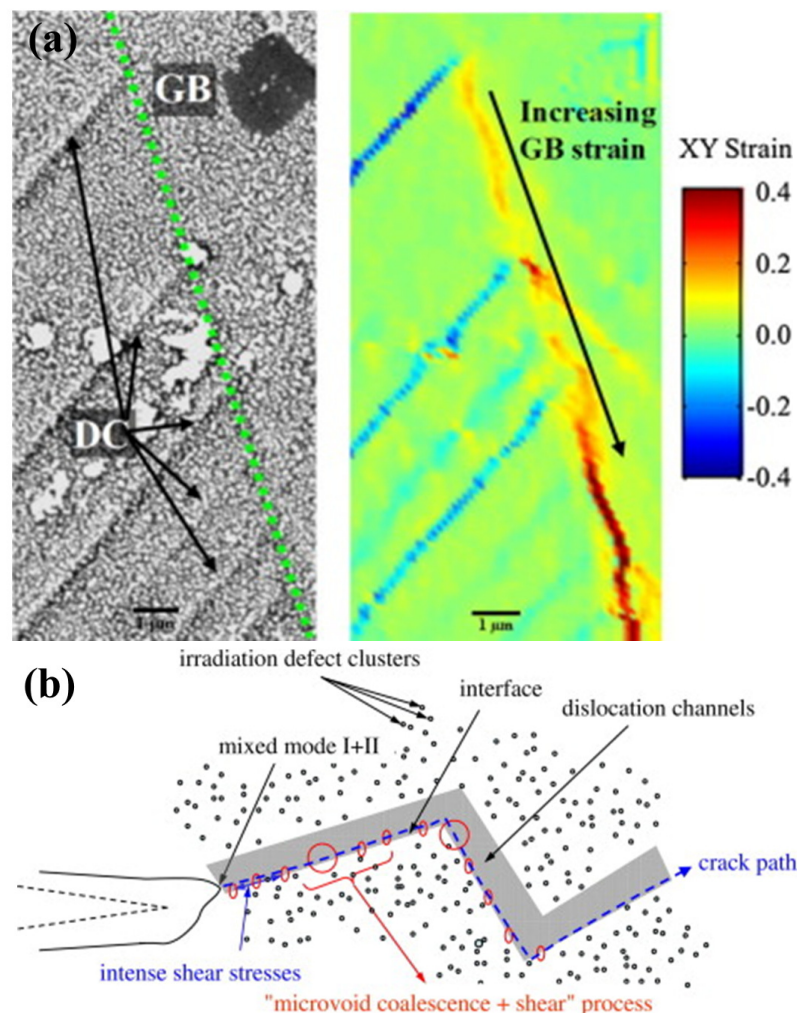


Figure 10. (color online) (a) The interaction between dislocation channels and grain boundaries that results in stress concentration due to the pile-up of dislocations by grain boundaries and transmission of dislocations through grain boundaries. (Reprinted with permission from [129]. Copyright 2015 by Elsevier.) (b) Illustration of the propagation of crack tip along the interface of dislocation channels. (Reprinted with permission from [130]. Copyright 2007 by Elsevier.)

Besides the interaction sites, the interface between defect-free channels and the adjacent irradiated matrix is also the latent position for the germination of microvoids. As illustrated in Figure 10b, the propagation of micro-cracks in the front region of a micro crack is presented in irradiated materials with defect-free channels [60]. Around the crack tip, the intense stress field can prompt the aggregation of vacancies into the interfaces which is similar to the case of grain boundaries, and thereby the accumulated microvoids can either facilitate the propagation of cracks along the interface of defect-free channels or the generation of sub-cracks connected to the original channels. It is generally believed that the generated defect-free channel is the most critical factor resulting in irradiation embrittlement and degradation of material properties.

5. Summary and Outlook

In this review, corresponding mechanisms for the phenomena of irradiation-hardening and embrittlement are overviewed, which include the formation of irradiation-induced defects, dislocation-defect interaction, and evolution of defects and dislocations. So far, a consensus has been reached that the irradiation-hardening mainly originates from the impediment of sliding dislocation by irradiation-induced defects, and the annihilation of irradiation defects leading to the formation of defect-free channels is the primary factor resulting in the irradiation embrittlement as microvoids tend to nucleate at the intersection sites of the channels and grain boundaries, as well as the interface of channels. In order to obtain a sophisticated comprehension of the fundamental mechanisms, persistent efforts are needed in the fields of numerical simulations, experimental observations and theoretical models, as the study of irradiation effect is intrinsically a multi-scale issue that ranges from atomic scale to micro scale and macro scale.

Funding: This work was supported by the National Nature Science foundation of China (NSFC) under Contract No. 11802344, and Natural Science Foundation of Hunan Province, China (Grant No. 2019JJ50809). X.Z. thanks the initial funding supported by Central South University.

Acknowledgments: The author acknowledges Duan, Chu and Terentyev for the useful discussion.

Conflicts of Interest: The author declares no conflict of interest. The funders had no role in the design of the study; in the collection, analyses, or interpretation of data; in the writing of the manuscript, or in the decision to publish the results.

References

1. Li, Q.; Shen, Y.; Zhu, J.; Huang, X.; Shang, Z. Evaluation of Irradiation Hardening of P92 Steel under Ar Ion Irradiation. *Metals* **2018**, *8*, 94. [[CrossRef](#)]
2. Bai, X.; Wu, S.; Liaw, P.K.; Shao, L.; Gigax, J. Effect of Heavy Ion Irradiation Dosage on the Hardness of SA508-IV Reactor Pressure Vessel Steel. *Metals* **2017**, *7*, 25. [[CrossRef](#)]
3. Jitsukawa, S.; Suzuki, K.; Okubo, N.; Ando, M.; Shiba, K. Irradiation effects on reduced activation ferritic/martensitic steels-tensile, impact, fatigue properties and modelling. *Nucl. Fusion* **2009**, *49*, 733–737. [[CrossRef](#)]
4. Alamo, A.; Horsten, M.; Averty, X.; Materna-Morris, E.I.; Rieth, M.; Brachet, J.C. Mechanical behavior of reduced-activation and conventional martensitic steels after neutron irradiation in the range 250–450 degrees C. *J. Nucl. Mater.* **2000**, *283*, 353–357. [[CrossRef](#)]
5. Hojna, A. Overview of Intergranular Fracture of Neutron Irradiated Austenitic Stainless Steels. *Metals* **2017**, *7*, 392. [[CrossRef](#)]
6. Li, M.; Sokolov, M.A.; Zinkle, S.J. Tensile and fracture toughness properties of neutron-irradiated CuCrZr. *J. Nucl. Mater.* **2009**, *393*, 36–46. [[CrossRef](#)]
7. Fabritsiev, S.A.; Pokrovsky, A.S. Effect of irradiation temperature on microstructure, radiation hardening and embrittlement of pure copper and copper-based alloy. *J. Nucl. Mater.* **2007**, *367*, 977–983. [[CrossRef](#)]
8. Sharma, G.; Mukherjee, P.; Chatterjee, A.; Gayathri, N.; Sarkar, A.; Chakravarty, J.K. Study of the effect of alpha irradiation on the microstructure and mechanical properties of nanocrystalline Ni. *Acta Mater.* **2013**, *61*, 3257–3266. [[CrossRef](#)]

9. Singh, B.N.; Horsewell, A.; Toft, P. Effects of neutron irradiation on microstructure and mechanical properties of pure iron. *J. Nucl. Mater.* **1999**, *271*, 97–101. [[CrossRef](#)]
10. Zinkle, S.J.; Singh, B.N. Microstructure of neutron-irradiated iron before and after tensile deformation. *J. Nucl. Mater.* **2006**, *351*, 269–284. [[CrossRef](#)]
11. Fukuda, M.; Hasegawa, A.; Tanno, T.; Nogami, S.; Kurishita, H. Property change of advanced tungsten alloys due to neutron irradiation. *J. Nucl. Mater.* **2013**, *442*, S273–S276. [[CrossRef](#)]
12. Cockeram, B.V.; Smith, R.W.; Leonard, K.J.; Byun, T.S.; Snead, L.L. Development of microstructure and irradiation hardening of Zircaloy during low dose neutron irradiation at nominally 358 degrees C. *J. Nucl. Mater.* **2011**, *418*, 46–61. [[CrossRef](#)]
13. Onimus, F.; Bechade, J.L.; Duguay, C.; Gilbon, D.; Pilvin, P. Investigation of neutron radiation effects on the mechanical behavior of recrystallized zirconium alloys. *J. Nucl. Mater.* **2006**, *358*, 176–189. [[CrossRef](#)]
14. Marmy, P.; Leguey, T. Impact of irradiation on the tensile and fatigue properties of two titanium alloys. *J. Nucl. Mater.* **2001**, *296*, 155–164. [[CrossRef](#)]
15. Li, M.; Byun, T.S.; Snead, L.L.; Zinkle, S.J. Low-temperature thermally-activated deformation and irradiation softening in neutron-irradiated molybdenum. *J. Nucl. Mater.* **2008**, *377*, 409–414. [[CrossRef](#)]
16. Chopra, O.K.; Rao, A.S. A review of irradiation effects on LWR core internal materials—IASCC susceptibility and crack growth rates of austenitic stainless steels. *J. Nucl. Mater.* **2011**, *409*, 235–256. [[CrossRef](#)]
17. Knaster, J.; Moeslang, A.; Muroga, T. Materials research for fusion. *Nat. Phys.* **2016**, *12*, 424–434. [[CrossRef](#)]
18. Song, C. Irradiation effects on Zr-2.5Nb in power reactors. *CNL Nucl. Rev.* **2016**, *5*, 17–36. [[CrossRef](#)]
19. Azevedo, C.R.F. A review on neutron-irradiation-induced hardening of metallic components. *Eng. Fail. Anal.* **2011**, *18*, 1921–1942. [[CrossRef](#)]
20. Singh, B.N.; Foreman, A.J.E.; Trinkaus, H. Radiation hardening revisited: Role of intracascade clustering. *J. Nucl. Mater.* **1997**, *249*, 103–115. [[CrossRef](#)]
21. Kuksenko, V.; Pareige, C.; Genevois, C.; Cuvilly, F.; Roussel, M.; Pareige, P. Effect of neutron-irradiation on the microstructure of a Fe-12at.%Cr alloy. *J. Nucl. Mater.* **2011**, *415*, 61–66. [[CrossRef](#)]
22. Kuksenko, V.; Pareige, C.; Pareige, P. Cr precipitation in neutron irradiated industrial purity Fe-Cr model alloys. *J. Nucl. Mater.* **2013**, *432*, 160–165. [[CrossRef](#)]
23. Byun, T.S.; Farrell, K.; Li, M. Deformation in metals after low-temperature irradiation: Part I—Mapping macroscopic deformation modes on true stress-dose plane. *Acta Mater.* **2008**, *56*, 1044–1055. [[CrossRef](#)]
24. Byun, T.S.; Farrell, K.; Li, M. Deformation in metals after low-temperature irradiation: Part II—Irradiation hardening, strain hardening, and stress ratios. *Acta Mater.* **2008**, *56*, 1056–1064. [[CrossRef](#)]
25. Chang, Y.; Zhang, J.; Li, X.; Guo, Q.; Wan, F.; Long, Y. Microstructure and nanoindentation of the CLAM steel with nanocrystalline grains under Xe irradiation. *J. Nucl. Mater.* **2014**, *455*, 624–629. [[CrossRef](#)]
26. Dai, Y.; Henry, J.; Tong, Z.; Averty, X.; Malaplate, J.; Long, B. Neutron/proton irradiation and He effects on the microstructure and mechanical properties of ferritic/martensitic steels T91 and EM10. *J. Nucl. Mater.* **2011**, *415*, 306–310. [[CrossRef](#)]
27. Suzudo, T.; Yamaguchi, M. Simulation of He embrittlement at grain boundaries in bcc transition metals. *J. Nucl. Mater.* **2015**, *465*, 695–701. [[CrossRef](#)]
28. Yang, Y.; Ding, J.; Zhang, H.; Zhang, P.; Mei, X.; Huang, S.; Zhao, J. Atomistic understanding of helium behaviors at grain boundaries in vanadium. *Comput. Mater. Sci.* **2019**, *158*, 296–306. [[CrossRef](#)]
29. Fan, H.; El-Awady, J.A.; Wang, Q. Towards further understanding of stacking fault tetrahedron absorption and defect-free channels—A molecular dynamics study. *J. Nucl. Mater.* **2015**, *458*, 176–186. [[CrossRef](#)]
30. Fan, H.; Wang, Q.; Ouyang, C. Comprehensive molecular dynamics simulations of the stacking fault tetrahedron interacting with a mixed dislocation at elevated temperature. *J. Nucl. Mater.* **2015**, *465*, 245–253. [[CrossRef](#)]
31. Xu, W.; Zhang, Y.; Cheng, G.; Jian, W.; Millett, P.C.; Koch, C.C.; Mathaudhu, S.N.; Zhu, Y. In-situ atomic-scale observation of irradiation-induced void formation. *Nat. Commun.* **2013**, *4*, 2288. [[CrossRef](#)] [[PubMed](#)]
32. Xiong, L.; Xu, S.; McDowell, D.L.; Chen, Y. Concurrent atomistic-continuum simulations of dislocation-void interactions in fcc crystals. *Int. J. Plast.* **2015**, *65*, 33–42. [[CrossRef](#)]
33. Traiviratana, S.; Bringa, E.M.; Benson, D.J.; Meyers, M.A. Void growth in metals: Atomistic calculations. *Acta Mater.* **2008**, *56*, 3874–3886. [[CrossRef](#)]
34. Cui, Y.; Po, G.; Ghoniem, N. Size-Tuned Plastic Flow Localization in Irradiated Materials at the Submicron Scale. *Phys. Rev. Lett.* **2018**, *120*, 215501. [[CrossRef](#)] [[PubMed](#)]

35. Cui, Y.; Po, G.; Ghoniem, N. A Coupled Dislocation Dynamics-Continuum Barrier Field Model with Application to Irradiated Materials. *Int. J. Plast.* **2018**, *104*, 54–67. [[CrossRef](#)]
36. Kumar, N.N.; Durgaprasad, P.V.; Dutta, B.K.; Dey, G.K. Modeling of radiation hardening in ferritic/martensitic steel using multi-scale approach. *Comput. Mater. Sci.* **2012**, *53*, 258–267. [[CrossRef](#)]
37. Patra, A.; McDowell, D.L. A void nucleation and growth based damage framework to model failure initiation ahead of a sharp notch in irradiated bcc materials. *J. Mech. Phys. Solids* **2015**, *74*, 111–135. [[CrossRef](#)]
38. Barton, N.R.; Arsenlis, A.; Marian, J. A polycrystal plasticity model of strain localization in irradiated iron. *J. Mech. Phys. Solids* **2013**, *61*, 341–351. [[CrossRef](#)]
39. Xiao, X.; Yu, L. Cross-sectional nano-indentation of ion-irradiated steels: Finite element simulations based on the strain-gradient crystal plasticity theory. *Int. J. Eng. Sci.* **2019**, *143*, 56–72. [[CrossRef](#)]
40. Xiao, X.; Chen, L.; Yu, L.; Duan, H. Modelling nano-indentation of ion-irradiated FCC single crystals by strain-gradient crystal plasticity theory. *Int. J. Plast.* **2019**, *111*, 135–151. [[CrossRef](#)]
41. Bacon, D.J.; Osetsky, Y.N. The atomic-scale modeling of dislocation-obstacle interactions in irradiated metals. *JOM* **2007**, *59*, 40–45. [[CrossRef](#)]
42. Bacon, D.J.; Osetsky, Y.N. Dislocation-Obstacle Interactions at Atomic Level in Irradiated Metals. *Math. Mech. Solids* **2009**, *14*, 270–283. [[CrossRef](#)]
43. Baudouin, J.B.; Nomoto, A.; Perez, M.; Monnet, G.; Domain, C. Molecular dynamics investigation of the interaction of an edge dislocation with Frank loops in Fe-Ni-10-Cr-20 alloy. *J. Nucl. Mater.* **2015**, *465*, 301–310. [[CrossRef](#)]
44. Di, S.; Yao, Z.; Daymond, M.R.; Zu, X.; Peng, S.; Gao, F. Dislocation-accelerated void formation under irradiation in zirconium. *Acta Mater.* **2015**, *82*, 94–99. [[CrossRef](#)]
45. Hayward, E.; Deo, C.; Uberuaga, B.P.; Tome, C.N. The interaction of a screw dislocation with point defects in bcc iron. *Philos. Mag.* **2012**, *92*, 2759–2778. [[CrossRef](#)]
46. Liu, Q.; Deng, L.; Wang, X. Interactions between prismatic dislocation loop and coherent twin boundary under nanoindentation investigated by molecular dynamics. *Mater. Sci. Eng. A-Struct. Mater. Prop. Microstruct. Process.* **2016**, *676*, 182–190. [[CrossRef](#)]
47. Ma, L.; Xiao, S.; Deng, H.; Hu, W. Atomistic simulation of mechanical properties and crack propagation of irradiated nickel. *Comput. Mater. Sci.* **2016**, *120*, 21–28. [[CrossRef](#)]
48. Dai, C.; Balogh, L.; Yao, Z.; Daymond, M.R. Atomistic simulations of the formation of <c>-component dislocation loops in alpha-zirconium. *J. Nucl. Mater.* **2016**, *478*, 125–134. [[CrossRef](#)]
49. Zhang, L.; Lu, C.; Tieu, K.; Su, L.; Zhao, X.; Pei, L. Stacking fault tetrahedron induced plasticity in copper single crystal. *Mater. Sci. Eng. A-Struct. Mater. Prop. Microstruct. Process.* **2017**, *680*, 27–38. [[CrossRef](#)]
50. Coppola, R.; Klimenkov, M. Dose Dependence of Micro-Voids Distributions in Low-Temperature Neutron Irradiated Eurofer97 Steel. *Metals* **2019**, *9*, 552. [[CrossRef](#)]
51. Stergar, E.; Eremin, S.G.; Gavrillov, S.; Lambrecht, M.; Makarov, O.; Iakovlev, V. Influence of LBE long term exposure and simultaneous fast neutron irradiation on the mechanical properties of T91 and 316L. *J. Nucl. Mater.* **2016**, *473*, 28–34. [[CrossRef](#)]
52. Fu, Z.Y.; Liu, P.P.; Wan, F.R.; Zhan, Q. Helium and hydrogen irradiation induced hardening in CLAM steel. *Fusion Eng. Des.* **2015**, *91*, 73–78. [[CrossRef](#)]
53. Bai, X.M.; Voter, A.F.; Hoagland, R.G.; Nastasi, M.; Uberuaga, B.P. Efficient Annealing of Radiation Damage Near Grain Boundaries via Interstitial Emission. *Science* **2010**, *327*, 1631–1634. [[CrossRef](#)] [[PubMed](#)]
54. Byun, T.S.; Hoelzer, D.T.; Kim, J.H.; Maloy, S.A. A comparative assessment of the fracture toughness behavior of ferritic-martensitic steels and nanostructured ferritic alloys. *J. Nucl. Mater.* **2017**, *484*, 157–167. [[CrossRef](#)]
55. Nakai, R.; Yabuuchi, K.; Nogami, S.; Hasegawa, A. The effect of voids on the hardening of body-centered cubic Fe. *J. Nucl. Mater.* **2016**, *471*, 233–238. [[CrossRef](#)]
56. Kudiiarov, V.N.; Larionov, V.V.; Tyurin, Y.I. Mechanical Property Testing of Hydrogenated Zirconium Irradiated with Electrons. *Metals* **2018**, *8*, 207. [[CrossRef](#)]
57. Saleh, M.; Zaidi, Z.; Hurt, C.; Ionescu, M.; Munroe, P.; Bhattacharyya, D. Comparative Study of Two Nanoindentation Approaches for Assessing Mechanical Properties of Ion-Irradiated Stainless Steel 316. *Metals* **2018**, *8*, 719. [[CrossRef](#)]
58. Ge, H.E.; Peng, L.; Dai, Y.; Huang, Q.Y.; Ye, M.Y. Tensile properties of CLAM steel irradiated up to 20.1 dpa in STIP-V. *J. Nucl. Mater.* **2016**, *468*, 240–245. [[CrossRef](#)]

59. Huang, H.F.; Li, J.J.; Li, D.H.; Liu, R.D.; Lei, G.H.; Huang, Q.; Yan, L. TEM, XRD and nanoindentation characterization of Xenon ion irradiation damage in austenitic stainless steels. *J. Nucl. Mater.* **2014**, *454*, 168–172. [[CrossRef](#)]
60. Victoria, M.; Baluc, N.; Bailat, C.; Dai, Y.; Luppó, M.I.; Schaublin, R.; Singh, B.N. The microstructure and associated tensile properties of irradiated fcc and bcc metals. *J. Nucl. Mater.* **2000**, *276*, 114–122. [[CrossRef](#)]
61. Madjasevic, M.; Alrriazouzi, A. Effect of Cr on the mechanical properties and microstructure of Fe-Cr model alloys after n-irradiation. *J. Nucl. Mater.* **2008**, *377*, 147–154. [[CrossRef](#)]
62. Robach, J.S.; Robertson, I.M.; Lee, H.J.; Wirth, B.D. Dynamic observations and atomistic simulations of dislocation-defect interactions in rapidly quenched copper and gold. *Acta Mater.* **2006**, *54*, 1679–1690. [[CrossRef](#)]
63. Matsukawa, Y.; Zinkle, S.J. Dynamic observation of the collapse process of a stacking fault tetrahedron by moving dislocations. *J. Nucl. Mater.* **2004**, *329*, 919–923. [[CrossRef](#)]
64. Xiao, X.; Chen, Q.; Yang, H.; Duan, H.; Qu, J. A mechanistic model for depth-dependent hardness of ion irradiated metals. *J. Nucl. Mater.* **2017**, *485*, 80–89. [[CrossRef](#)]
65. Sharma, G.; Sarkar, A.; Varshney, J.; Ramamurty, U.; Kumar, A.; Gupta, S.K.; Chakravartty, J.K. Effect of irradiation on the microstructure and mechanical behavior of nanocrystalline nickel. *Scr. Mater.* **2011**, *65*, 727–730. [[CrossRef](#)]
66. Liu, W.B.; Ji, Y.Z.; Tan, P.K.; Zhang, C.; He, C.H.; Yang, Z.G. Microstructure evolution during helium irradiation and post-irradiation annealing in a nanostructured reduced activation steel. *J. Nucl. Mater.* **2016**, *479*, 323–330. [[CrossRef](#)]
67. Chen, C.L.; Richter, A.; Koenigler, R. The effect of dual Fe⁺/He⁺ ion beam irradiation on microstructural changes in FeCrAl ODS alloys. *J. Alloy. Compd.* **2014**, *586*, S173–S179. [[CrossRef](#)]
68. Jin, S.; Guo, L.; Li, T.; Chen, J.; Yang, Z.; Luo, F.; Tang, R.; Qiao, Y.; Liu, F. Microstructural evolution of P92 ferritic/martensitic steel under Ar⁺ ion irradiation at elevated temperature. *Mater. Charact.* **2012**, *68*, 63–70. [[CrossRef](#)]
69. Eldrup, M.; Singh, B.N.; Zinkle, S.J.; Byun, T.S.; Farrell, K. Dose dependence of defect accumulation in neutron irradiated copper and iron. *J. Nucl. Mater.* **2002**, *307*, 912–917. [[CrossRef](#)]
70. Jin, S.X.; Guo, L.P.; Yang, Z.; Fu, D.J.; Liu, C.S.; Xiao, W.; Tang, R.; Liu, F.H.; Qiao, Y.X. Microstructural evolution in nickel alloy C-276 after Ar⁺ ion irradiation. *Nucl. Instrum. Methods Phys. Res. Sect. B-Beam Interact. Mater. Atoms* **2011**, *269*, 209–215. [[CrossRef](#)]
71. Hu, X.; Koyanagi, T.; Fukuda, M.; Katoh, Y.; Snead, L.L.; Wirth, B.D. Defect evolution in single crystalline tungsten following low temperature and low dose neutron irradiation. *J. Nucl. Mater.* **2016**, *470*, 278–289. [[CrossRef](#)]
72. Schaublin, R.; Ramar, A.; Baluc, N.; de Castro, V.; Monge, M.A.; Leguey, T.; Schmid, N.; Bonjour, C. Microstructural development under irradiation in European ODS ferritic/martensitic steels. *J. Nucl. Mater.* **2006**, *351*, 247–260. [[CrossRef](#)]
73. Materna-Morris, E.; Lindau, R.; Schneider, H.C.; Moeslang, A. Tensile behavior of EUROFER ODS steel after neutron irradiation up to 16.3 dpa between 250 and 450 degrees C. *Fusion Eng. Des.* **2015**, *98–99*, 2038–2041. [[CrossRef](#)]
74. Tanigawa, H.; Sakasegawa, H.; Hashimoto, N.; Klueh, R.L.; Ando, M.; Sokolov, M.A. Irradiation effects on precipitation and its impact on the mechanical properties of reduced-activation ferritic/martensitic steels. *J. Nucl. Mater.* **2007**, *367*, 42–47. [[CrossRef](#)]
75. Madjasevic, M.; Lucon, E.; Almazouzi, A. Behavior of ferritic/martensitic steels after n-irradiation at 200 and 300 degrees C. *J. Nucl. Mater.* **2008**, *377*, 101–108. [[CrossRef](#)]
76. Klimenkov, M.; Materna-Morris, E.; Moeslang, A. Characterization of radiation induced defects in EUROFER 97 after neutron irradiation. *J. Nucl. Mater.* **2011**, *417*, 124–126. [[CrossRef](#)]
77. Jin, H.H.; Shin, C.; Kim, D.H.; Oh, K.H.; Kwon, J.H. Irradiation induced dislocation loop and its influence on the hardening behavior of Fe-Cr alloys by an Fe ion irradiation. *Nucl. Instrum. Methods Phys. Res. Sect. B-Beam Interact. Mater. Atoms* **2008**, *266*, 4845–4848. [[CrossRef](#)]
78. Etienne, A.; Hernandez-Mayoral, M.; Genevois, C.; Radiguet, B.; Pareige, P. Dislocation loop evolution under ion irradiation in austenitic stainless steels. *J. Nucl. Mater.* **2010**, *400*, 56–63. [[CrossRef](#)]
79. Yao, B.; Edwards, D.J.; Kurtz, R.J. TEM characterization of dislocation loops in irradiated bcc Fe-based steels. *J. Nucl. Mater.* **2013**, *434*, 402–410. [[CrossRef](#)]

80. Kai, J.J.; Kulcinski, G.L. 14 MeV nickel-ion irradiated HT-9 ferritic steel with and without helium preimplantation. *J. Nucl. Mater.* **1990**, *175*, 227–236. [[CrossRef](#)]
81. Wang, K.; Dai, Y.; Spaetig, P. Microstructure and fracture behavior of F82H steel under different irradiation and tensile test conditions. *J. Nucl. Mater.* **2016**, *468*, 246–254. [[CrossRef](#)]
82. Li, M.; Eldrup, M.; Byun, T.S.; Hashimo, N.; Snead, L.L.; Zinkle, S.J. Low temperature neutron irradiation effects on microstructure and tensile properties of molybdenum. *J. Nucl. Mater.* **2008**, *376*, 11–28. [[CrossRef](#)]
83. Yamashita, S.; Tachi, Y.; Akasaka, N.; Nishinoiri, K.; Takahashi, H. Effect of neutron irradiation on the microstructure of modified SUS316 stainless steels. *J. Nucl. Mater.* **2011**, *417*, 953–957. [[CrossRef](#)]
84. Fukuda, M.; Hasegawa, A.; Nogami, S.; Yabuuchi, K. Microstructure development of dispersion-strengthened tungsten due to neutron irradiation. *J. Nucl. Mater.* **2014**, *449*, 213–218. [[CrossRef](#)]
85. Zhang, T.; Vieh, C.; Wang, K.; Dai, Y. Irradiation-induced evolution of mechanical properties and microstructure of Eurofer 97. *J. Nucl. Mater.* **2014**, *450*, 48–53. [[CrossRef](#)]
86. Getto, E.; Jiao, Z.; Monterrosa, A.M.; Sun, K.; Was, G.S. Effect of irradiation mode on the microstructure of self-ion irradiated ferritic-martensitic alloys. *J. Nucl. Mater.* **2015**, *465*, 116–126. [[CrossRef](#)]
87. Kolluri, M.; Edmondson, P.D.; Luzginova, N.V.; Vander Berg, F.A. Influence of irradiation temperature on microstructure of EU batch of ODS Eurofer97 steel irradiated with neutrons. *Mater. Sci. Technol.* **2014**, *30*, 1697–1703. [[CrossRef](#)]
88. Klimenkov, M.; Moeslang, A.; Materna-Morris, E. Helium influence on the microstructure and swelling of 9%Cr ferritic steel after neutron irradiation to 16.3 dpa. *J. Nucl. Mater.* **2014**, *453*, 54–59. [[CrossRef](#)]
89. Cockeram, B.V.; Smith, R.W.; Hashimoto, N.; Snead, L.L. The swelling, microstructure, and hardening of wrought LCAC, TZM, and ODS molybdenum following neutron irradiation. *J. Nucl. Mater.* **2011**, *418*, 121–136. [[CrossRef](#)]
90. Heintze, C.; Bergner, F.; Akhmadaliev, S.; Altstadt, E. Ion irradiation combined with nanoindentation as a screening test procedure for irradiation hardening. *J. Nucl. Mater.* **2016**, *472*, 196–205. [[CrossRef](#)]
91. Kasada, R.; Konishi, S.; Yabuuchi, K.; Nogami, S.; Ando, M.; Hamaguchi, D.; Tanigawa, H. Depth-dependent nanoindentation hardness of reduced-activation ferritic steels after MeV Fe-ion irradiation. *Fusion Eng. Des.* **2014**, *89*, 1637–1641. [[CrossRef](#)]
92. Dunn, A.; Dingreville, R.; Martinez, E.; Capolungo, L. Identification of dominant damage accumulation processes at grain boundaries during irradiation in nanocrystalline alpha-Fe: A statistical study. *Acta Mater.* **2016**, *110*, 306–323. [[CrossRef](#)]
93. Chen, Y.; Li, N.; Bufford, D.C.; Li, J.; Hattar, K.; Wang, H.; Zhang, X. In situ study of heavy ion irradiation response of immiscible Cu/Fe multilayers. *J. Nucl. Mater.* **2016**, *475*, 274–279. [[CrossRef](#)]
94. Chen, Y.; Li, J.; Yu, K.Y.; Wang, H.; Kirk, M.A.; Li, M.; Zhang, X. In situ studies on radiation tolerance of nanotwinned Cu. *Acta Mater.* **2016**, *111*, 148–156. [[CrossRef](#)]
95. Yu, K.Y.; Bufford, D.; Sun, C.; Liu, Y.; Wang, H.; Kirk, M.A.; Li, M.; Zhang, X. Removal of stacking-fault tetrahedra by twin boundaries in nanotwinned metals. *Nat. Commun.* **2013**, *4*, 1377. [[CrossRef](#)]
96. Liu, W.; Ji, Y.; Tan, P.; Zang, H.; He, C.; Yun, D.; Zhang, C.; Yang, Z. Irradiation Induced Microstructure Evolution in Nanostructured Materials: A Review. *Materials* **2016**, *9*, 105. [[CrossRef](#)]
97. Singh, B.N.; Edwards, D.J.; Toft, P. Effects of neutron irradiation on mechanical properties and microstructures of dispersion and precipitation hardened copper alloys. *J. Nucl. Mater.* **1996**, *238*, 244–259. [[CrossRef](#)]
98. Shi, X.J.; Dupuy, L.; Devincere, B.; Terentyev, D.; Vincent, L. Interaction of < 100 > dislocation loops with dislocations studied by dislocation dynamics in alpha-iron. *J. Nucl. Mater.* **2015**, *460*, 37–43. [[CrossRef](#)]
99. Bachhav, M.; Yao, L.; Odette, G.R.; Marquis, E.A. Microstructural changes in a neutron-irradiated Fe-6 at.%Cr alloy. *J. Nucl. Mater.* **2014**, *453*, 334–339. [[CrossRef](#)]
100. Kuksenko, V.; Pareige, C.; Pareige, P. Intra granular precipitation and grain boundary segregation under neutron irradiation in a low purity Fe-Cr based alloy. *J. Nucl. Mater.* **2012**, *425*, 125–129. [[CrossRef](#)]
101. Jiao, Z.; Was, G.S. Novel features of radiation-induced segregation and radiation-induced precipitation in austenitic stainless steels. *Acta Mater.* **2011**, *59*, 1220–1238. [[CrossRef](#)]
102. Parish, C.M.; White, R.M.; LeBeau, J.M.; Miller, M.K. Response of nanostructured ferritic alloys to high-dose heavy ion irradiation. *J. Nucl. Mater.* **2014**, *445*, 251–260. [[CrossRef](#)]
103. Sauzay, M.; Vor, K. Influence of plastic slip localization on grain boundary stress fields and microcrack nucleation. *Eng. Fract. Mech.* **2013**, *110*, 330–349. [[CrossRef](#)]

104. Osetsky, Y.N.; Serra, A.; Priego, V. Interactions between mobile dislocation loops in Cu and alpha-Fe. *J. Nucl. Mater.* **2000**, *276*, 202–212. [[CrossRef](#)]
105. Osetsky, Y.N.; Bacon, D.J.; Serra, A.; Singh, B.N.; Golubov, S.I. One-dimensional atomic transport by clusters of self-interstitial atoms in iron and copper. *Philos. Mag.* **2003**, *83*, 61–91. [[CrossRef](#)]
106. Xiao, X.; Song, D.; Xue, J.; Chu, H.; Duan, H. A size-dependent tensorial plasticity model for FCC singlecrystal with irradiation. *Int. J. Plast.* **2015**, *65*, 152–167. [[CrossRef](#)]
107. Xiao, X.; Song, D.; Xue, J.; Chu, H.; Duana, H. A self-consistent plasticity theory for modeling the thermo-mechanical properties of irradiated FCC metallic polycrystals. *J. Mech. Phys. Solids* **2015**, *78*, 1–16. [[CrossRef](#)]
108. Yang, S.; Yang, Z.; Wang, H.; Watanabe, S.; Shibayama, T. Effect of laser and/or electron beam irradiation on void swelling in SUS316L austenitic stainless steel. *J. Nucl. Mater.* **2017**, *488*, 215–221. [[CrossRef](#)]
109. Fabritsiev, S.A.; Pokrovsky, A.S. Effect of irradiation temperature and dose on radiation hardening of some pure metals. *J. Nucl. Mater.* **2011**, *417*, 940–943. [[CrossRef](#)]
110. Brimbal, D.; Decamps, B.; Barbu, A.; Meslin, E.; Henry, J. Dual-beam irradiation of alpha-iron: Heterogeneous bubble formation on dislocation loops. *J. Nucl. Mater.* **2011**, *418*, 313–315. [[CrossRef](#)]
111. Briceno, M.; Kacher, J.; Robertson, I.M. Dynamics of dislocation interactions with stacking-fault tetrahedra at high temperature. *J. Nucl. Mater.* **2013**, *433*, 390–396. [[CrossRef](#)]
112. Matsukawa, Y.; Osetsky, Y.N.; Stoller, R.E.; Zinkle, S.J. Mechanisms of stacking fault tetrahedra destruction by gliding dislocations in quenched gold. *Philos. Mag.* **2008**, *88*, 581–597. [[CrossRef](#)]
113. Rodney, D. Atomic-scale modeling of clear band formation in FCC metals. *Nucl. Instrum. Methods Phys. Res. Sect. B-Beam Interact. Mater. Atoms* **2005**, *228*, 100–110. [[CrossRef](#)]
114. Matsukawa, Y.; Osetsky, Y.N.; Stoller, R.E.; Zinkle, S.J. Destruction processes of large stacking fault tetrahedra induced by direct interaction with gliding dislocations. *J. Nucl. Mater.* **2006**, *351*, 285–294. [[CrossRef](#)]
115. Matsukawa, Y.; Osetsky, Y.N.; Stoller, R.E.; Zinkle, S.J. The collapse of stacking-fault tetrahedra by interaction with gliding dislocations. *Mater. Sci. Eng. A-Struct. Mater. Prop. Microstruct. Process.* **2005**, *400*, 366–369. [[CrossRef](#)]
116. Osetsky, Y.N.; Rodney, D.; Bacon, D.J. Atomic-scale study of dislocation-stacking fault tetrahedron interactions. Part I: Mechanisms. *Philos. Mag.* **2006**, *86*, 2295–2313. [[CrossRef](#)]
117. Kacher, J.; Cui, B.; Robertson, I.M. In situ and tomographic characterization of damage and dislocation processes in irradiated metallic alloys by transmission electron microscopy. *J. Mater. Res.* **2015**, *30*, 1202–1213. [[CrossRef](#)]
118. Byun, T.S.; Hashimoto, N.; Farrell, K.; Lee, E.H. Characteristics of microscopic strain localization in irradiated 316 stainless steels and pure vanadium. *J. Nucl. Mater.* **2006**, *349*, 251–264. [[CrossRef](#)]
119. Edwards, D.J.; Singh, B.N.; Bilde-Sorensen, J.B. Initiation and propagation of cleared channels in neutron-irradiated pure copper and a precipitation hardened CuCrZr alloy. *J. Nucl. Mater.* **2005**, *342*, 164–178. [[CrossRef](#)]
120. Nogami, S.; Sato, Y.; Hasegawa, A. Fatigue Crack Initiation in Proton-Irradiated Austenitic Stainless Steel. *J. Nucl. Sci. Technol.* **2011**, *48*, 1265–1271. [[CrossRef](#)]
121. Jiao, Z.; Was, G.S. Impact of localized deformation on IASCC in austenitic stainless steels. *J. Nucl. Mater.* **2011**, *408*, 246–256. [[CrossRef](#)]
122. Onimus, F.; Monnet, I.; Bechade, J.L.; Prioul, C.; Pilvin, P. A statistical TEM investigation of dislocation channeling mechanism in neutron irradiated zirconium alloys. *J. Nucl. Mater.* **2004**, *328*, 165–179. [[CrossRef](#)]
123. Mahajan, S.; Eyre, B.L. Formation of dislocation channels in neutron irradiated molybdenum. *Acta Mater.* **2017**, *122*, 259–265. [[CrossRef](#)]
124. Patra, A.; McDowell, D.L. Crystal plasticity investigation of the microstructural factors influencing dislocation channeling in a model irradiated bcc material. *Acta Mater.* **2016**, *110*, 364–376. [[CrossRef](#)]
125. Robertson, I.M.; Beaudoin, A.; Al-Fadhalah, K.; Chun-Ming, L.; Robach, J.; Wirth, B.D.; Arsenlis, A.; Ahn, D.; Sofronis, P. Dislocation-obstacle interactions: Dynamic experiments to continuum modeling. *Mater. Sci. Eng. A-Struct. Mater. Prop. Microstruct. Process.* **2005**, *400*, 245–250. [[CrossRef](#)]
126. de la Rubia, T.D.; Zbib, H.M.; Khraishi, T.A.; Wirth, B.D.; Victoria, M.; Caturla, M.J. Multiscale modelling of plastic flow localization in irradiated materials. *Nature* **2000**, *406*, 871–874. [[CrossRef](#)] [[PubMed](#)]
127. Kacher, J.; Liu, G.S.; Robertson, I.M. In situ and tomographic observations of defect free channel formation in ion irradiated stainless steels. *Micron* **2012**, *43*, 1099–1107. [[CrossRef](#)]

128. McMurtrey, M.D.; Was, G.S.; Patrick, L.; Farkas, D. Relationship between localized strain and irradiation assisted stress corrosion cracking in an austenitic alloy. *Mater. Sci. Eng. A-Struct. Mater. Prop. Microstruct. Process.* **2011**, *528*, 3730–3740. [[CrossRef](#)]
129. McMurtrey, M.D.; Cui, B.; Robertson, I.; Farkas, D.; Was, G.S. Mechanism of dislocation channel-induced irradiation assisted stress corrosion crack initiation in austenitic stainless steel. *Curr. Opin. Solid State Mater. Sci.* **2015**. [[CrossRef](#)]
130. Chaouadi, R. Effect of irradiation-induced plastic flow localization on ductile crack resistance behavior of a 9%Cr tempered martensitic steel. *J. Nucl. Mater.* **2008**, *372*, 379–390. [[CrossRef](#)]



© 2019 by the author. Licensee MDPI, Basel, Switzerland. This article is an open access article distributed under the terms and conditions of the Creative Commons Attribution (CC BY) license (<http://creativecommons.org/licenses/by/4.0/>).